Proceedings World Geothermal Congress 2020+1
Reykjavik, Iceland, April - October 2021

Permeability Obtained by Digital Analysis and Lattice-Boltzmann Method: Liquiñe Geothermal Area as case study, Southern Volcanic Zone (39ºS, Chile)

Eduardo Molina[a,b,c,*], Gloria Arancibia[a,b,c], Josefa Sepúlveda[a,b], Tomás Roquer[a,b], Diego Morata[b,d]

[a] Departamento de Ingeniería Estructural y Geotécnica, Pontificia Universidad Católica de Chile, Av. Vicuña Mackenna 4860, Macul, Santiago, Chile.

[b] Centro de Excelencia en Geotermia de los Andes (CEGA, FONDAP-CONICYT), Universidad de Chile, Plaza Ercilla 803, Santiago, Chile.

[c] Centro de Investigación en Nanotecnología y Materiales Avanzados (CIEN-UC), Pontificia Universidad Católica de Chile, Av. Vicuña Mackenna 4860, Macul, Santiago, Chile.

[d] Departamento de Geología, Universidad de Chile, Plaza Ercilla 803, Santiago, Chile.

[*] Corresponding author: eduardo.molina@ing.puc.cl

Keywords: Crystalline rocks, secondary permeability, Lattice-Boltzmann method, fluid flow simulations

ABSTRACT

Permeability is one of the most important factors which controls the occurrence of the geothermal resource because it represents the capacity of a rock to store and transmit hot fluids. When primary porosity governs the system, the approach to understand the hydraulic behaviour of the permeable media is usually based on the Darcy's Law; however, fractured media is more complex to analyse due to the interaction between fractures and faults that can mainly allow the pathway for the fluid flow, among other aspects. Furthermore, these discontinuities can be conditioned by both intrinsic properties of host rocks (e.g. crystals size, mineralogy, preferential orientation of crystals) and external factor (stress field, temperature, pore pressure). In this sense, previous studies have shown that the problem related to characterising fracture permeability can be partially solved by laboratory experiments under in-situ pressure and temperature conditions (geo-mechanical response) and under saturated conditions (hydro-mechanical response) complemented with the use of X-Ray microComputed Tomography (XR-μCT). This non-destructive method allows to examine the evolution of some petrophysical properties and also measure the porous system (e.g. fracture network). These results can be modelled and interpreted by the different numerical model used in the computational fluid dynamic (CFD) to solve problems related to the permeability. In recent years, Lattice Boltzmann Methods (LBM) turned into a fundamental tool in the simulation including both simple to complex multi-physical problems (e.g. heat transfer, fluid dynamics, multicomponent interactions). We selected the area surrounding Liquiñe, located at Southern Volcanic Zone (39 ºS, Chile), because it represents an excellent case of study of a fractured geothermal system hosted in crystalline rocks (mainly granitoids) affected by active faults of the Liquiñe Ofqui Fault System (LOFS) and Andean Transverse Faults (ATF), and the hot springs presented in this area are spatially controlled by the interaction of these faults. Because, there are not drill-holes data in this zone, to improve the knowledge about the circulation of hot fluids in the Liquiñe fractured geothermal system, petrophysical studies and modelling of fracture permeability were carried out in this study. For this, "healthy" samples of granodiorite from the outcrop were collected and were characterised by XR-mCT. After samples were heated at 25 ºC (room conditions), 150 ºC and 210 ºC, and mechanically tested in the laboratory to generate fractures. The temperatures were selected based on the estimated value by previous authors for this geothermal system. A digital analysis was carried out to measure the percentage of mineralogy and porosity and their distribution along with the cylindrical samples and the main parameters related to fractures, such as their length, aperture and tortuosity. The hydraulic parameters were established from both the digital analysis and digital rock model by means of the Cubic Law, Kozeny-Carman relation and Lattice-Boltzmann method. The results obtained mainly shown that when the temperature is increased the mean aperture decrease, but the tortuosity remains similar. About the value of the fracture permeability, it increases by several orders of magnitude with respect to the "healthy sample" but not between the non-heated and heated and fractured samples. Finally, this aspect may assume that the circulation of hot fluids in depth may occur under test conditions similar to those natural to this geothermal system.

1. INTRODUCTION

Unconventional geothermal systems are mainly characterised by to be hosted in rocks where the circulation of fluids, whether cold or hot, is due to the presence of fractured and interconnected zones. This fracturing of the rock bodies occurs as a response to external factors, mainly to stress regimes. Therefore, this permeability is referred to as "secondary permeability", as opposed to primary permeability, which responds to the original porosity of the rock (Gudmundsson, 2011). Therefore, the development of fracture networks allows the presence of geothermal systems in crystalline or tight rocks (e.g. granitoids, gneisses, limestones) since the primary porosity of these is very low or practically non-existent. Another external factor that can play an important role in the development of the fracture network is temperature because it can affect the rate of nucleation and growth of cracks, induced by the stress generated by the expansion of the crystals (Griffiths et al., 2016).

The study of the permeability of any medium (porous or fractured) is usually done through the analysis of data obtained from wells, where directly, or indirectly with geophysical methods, this parameter can be measured in addition to others of interest for the exploitation of geothermal systems, such as the distribution of the temperature, the storage capacity, the movement of the geothermal fluids, the recharge and discharge zones or, evidently, the own variation of the permeability in-depth (Ebigbo et al., 2016). However, when this information is not available, laboratory tests and mathematical-theoretical approaches constitute a set of tools with great

potential to perform analogous models to the natural system, by establishing similar test conditions (pressure, fluid pore pressure, temperature) to those that may occur in the system (Violay et al., 2017).

Laboratory approaches allow to know and determine the evolution of petrophysical properties, such as porosity or capillarity, depending on the applied stress, either thermal or mechanical or a combination of both and the effect on permeability (Cloetingh and Van Wees, 2017). On the other hand, the digital analysis of images from optical or electronic microscopies as well as the X-Ray microComputed Tomography allows obtaining information about the features of the fracture network. And the use of this last technique is especially interesting because it offers information in both 2D and 3D; besides that, it is a non-destructive method, so that the analysed sample is not lost and could be analysed again under other test conditions.

One of the most important parameters to estimate the permeability is the fracture aperture because it physically affects the circulation of fluids and mathematically allows approximations to the natural system from empirical data, for example the widely used Cubic Law and Kozeny-Carman relation (Hommel et al., 2017). Therefore, the determination of this parameter, together with others that are relevant to calculate the permeability in fractures, such as roughness, tortuosity, length, orientation, density, connectivity, etc., will allow to make analogous models of the system. In addition, these parameters can be modelled and interpreted by the different numerical model used in the computational fluid dynamic (CFD) to solve problems related to the permeability. In regard to CFD, Lattice Boltzmann Methods (LBM) turned into a fundamental tool in the fluid flow simulations (Yang et al., 2018).

The Liquiñe area has an especial interest due to there is a high amount of hot springs hosted in crystalline rocks and are related spatially with two main groups of faults (the Liquiñe-Ofqui Fault System -LOFS- and Andean Transverse Faults -ATF-). However, in spite of its potential, both scientific and energetic, it has not yet been studied in depth. Therefore, the aim of this work is to study by means of the digital analysis and the digital rock model how the combined effect of the thermal damage at low temperatures (< 210 ºC) and mechanically stresses, to allow the pathway to fluid flow through in an artificially fractured granodiorite host rock of the geothermal system in Liquiñe. To do that, after the heat the rock samples, they were loaded until their failure. Then, the fracture features were analysed by digital analysis and digital rock model to obtain the value of aperture, porosity, tortuosity and a 3D model of the fractures, which were mainly used to calculate permeability by the Cubic Law, the Kozeny-Carman relation and Lattice Boltzmann Method to reach analogous values of this natural and fractured geothermal system.

2. GEOLOGICAL CONTEXT AND SELECTED MATERIAL

2.1. Geology Related to the Liquiñe Geothermal System

Several hot spring manifestations characterise the Liquiñe geothermal system, placed in the Southern Volcanic Zone (SVZ) in Chile (39°S latitude) (Figure 1-a and b). The hot springs are spatially related to two main groups of faults, the Liquiñe-Ofqui Fault System (LOFS) and the Andean Transverse Faults (ATF) (e.g. Cembrano and Lara, 2009; Pérez-Flores et al., 2016). The first one is mainly composed by N-S lineaments and secondary NE strike-slip trending faults, and the second one by NW strike-slip trending faults. These manifestations are also related to the crystalline country rocks such as granitoids (basically granodiorites and tonalites) aged between Jurassic-Cretaceous and Miocene. These plutons are intruding to the Palaeozoic metamorphic rocks (gneiss and mylonitic gneisses); whereas Quaternary volcanic rocks and unconsolidated sediments are topographically disposed in the high and low parts, respectively (Lara and Moreno, 2004).

Previous studies showed that temperature of these hot springs is between 35 to 80 ºC, and their isotopic signal suggested that this natural system is placed at shallow depth (less than 3 Km) with a low to medium temperature (max. 200 ºC) (e.g. Sanchez et al., 2013; Held et al., 2018).

2.2. Miocene Granodiorite

For this study, samples of the Miocene granodiorite were collected from a quarry called “Cachim” in Liquiñe town (Figure 1-b, light blue star). In this outcrop, the granodiorite is cut by faults, dykes and fractures. These fractures can be open or partial to totally fill with main epidote. The measured spatial distribution of the fractures shown a representative value of 5 to 10 fractures per square meter and an averaged spacing between them, of 10 to 20 cm.

Petrographically, this granodiorite is a phaneritic medium-grained (0.2 to 3 mm in size) with a similar proportion of quartz and plagioclase (≤ 60%), K-feldspar (≤ 30%) and sparse biotite (≤ 10%). Some pieces of evidence of low-hydrothermal alteration are recognised by the presence of clays minerals in feldspars, and veinlets filled with epidote (±chlorite) and the effect of the tectonic processes can be inferred by the undulatory extinction of quartz crystals.

Cylindrical-shaped samples (1 cm in diameter and 2.5 cm in height) were drilled from a “fresh” block. For that, a core drill equipped with a diamond-covered edge bit was used, and all obtained samples were taken with the same orientation respect to their original position. To carry out the artificial fractures, these samples were polished until they were 2.5 ± 0.05 cm in length with flat and parallel faces, with a size ratio of 2.5:1 as technical standard suggest (e.g., ASTM or UNE-EN).

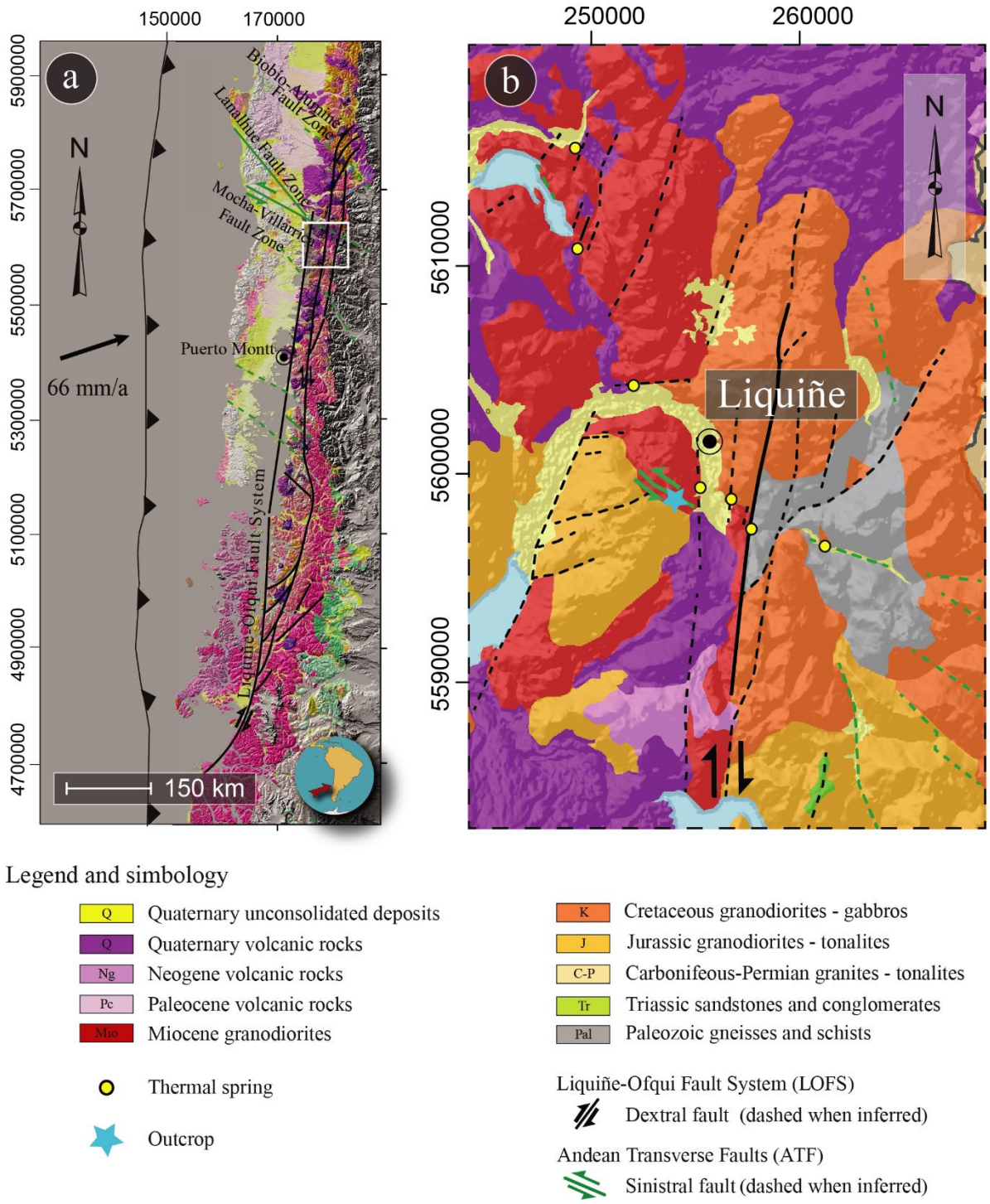

Figure 1: a) Regional geological map of the Southern Volcanic Zone, where the oblique subduction is 66 mm/yr, and the volcanic arc basement is indicated in pink. b) Geological map of Liquiñe, the light blue star indicates the selected outcrop "Cachim". The maps were modified from Lara and Moreno (2004), Rossenau et al. (2006), Sánchez et al. (2013) and Pérez-Flores et al. (2016).

3. METHODOLOGY

3.1. Thermal and Mechanical Treatment to Produce Artificial Fractures

Three different sets of cylindrical samples were prepared. One of them was heated at 150 ºC and other at 210 ºC. The last sample was not heated, and it served as a control to check the initial properties without heat treatment and to compare this original values respect to the variation on heated samples of their petrophysical properties and especially, differences about the fracture features. Samples were heated in a ventilated oven using a heating ramp of 6 ºC/min, and when the temperature was reached, it was maintained for 4 h to obtain a homogeneous temperature along with the whole sample. After that, samples were cooled inside the oven until room temperature to avoid any additional damage related to a quick cooling.

After that, all samples were loaded by means of a uniaxial compression test until their failure. A 50-C5632 machine (Controls) was used (Geotechnical Laboratory, Departamento de Ingeniería Estructural y Geotécnica, Pontificia Universidad Católica de Chile), applying a rate of 0.5 MPa/s. Strain gauges (model LY4x) were provided by the HBM company and were used to measure the strain and to corroborate the moment of failure.

Due to the small size of the samples and, also, to keep the samples as complete as possible to analyse by means of X-ray microcomputerized tomography, weak masking tape was applied around samples to avoid the detachment of fragments.

3.2. Digital Reconstruction and Postprocessing: Digital Properties

3.2.1 Enhancement and Postprocessing Procedures

To scan the samples by means of X-ray microComputerized Tomography (XR-μCT), a Bruker model SkyScan 1272 was used, and the applied conditions are summarized in Table 1. This equipment is located in the Department of Chemical and Bioprocess Engineering at Pontificia Universidad Católica de Chile. Samples were scanned before and after to apply the heat treatment, and also, after to produce the artificial fractures. In this way, the initial state of this rock and the effect of the temperature could be characterised, and subsequently, the result after loading them.

Table 1: Summarized scanning condition of XR-μCT.

Equip. model	SkyScan 1272	**Filter**	Aluminium 0.25 mm
Voltage/current	80 Kv/ 125 μA	**Image resolution**	6.0 μm
Exposure time	1500 ms	**Scanning time**	3h54'
Rotation step	0.5º	**Nº slices reconstructed**	1204
Image averaging	12	**Sample size = VOI**	10x10x0.7 mm^3

After the reconstruction of the raw data with NRecon software, and for enhancing the quality of every stack of images (n = 1204), an Anisotropic Diffusion Filter (ADF) was applied. This filter allows better preservation of the edges meanwhile the contrast is increased because only modified the value of a voxel if the difference respect to its six neighbours does not exceed the diffusion stop criteria (Cid et al., 2017). The whole process of improvement, segmentation and digital analysis was carried out with the software FIJI *v.1.52b* (Schindelin et al., 2012), a modified version of the original ImageJ software.

3.2.2 Digital Properties: Porosity and Aperture

The segmentation of the fractures (pore space) was carried out after binarised the images. From this segmentation, the percentage of porosity of the fractures (P_f, in %) was obtained as the relation between the volume of the fracture with respect to the total volume of the sample analysed, and the total related area of the fracture (S, in m^2).

On the other hand, to calculate the aperture of the fractures (e), it was used the Local Thickness plugin (Dougherty and Kunzelmann, 2007). This plugin considers the aperture as the diameter of the largest sphere that can be accommodated along all the fracture, and the results obtained consist of the frequency for each sphere of diameter d in the volume. In addition, we partially modified the code to obtain from the aperture results in 3D, the values of the aperture by the slice in 2D and know this distribution throughout the entire sample.

3.3. Fracture permeability

3.3.1 Cubic Law and Kozeny-Carman Relation

These approximations are two of the most used non-empirical models for permeability. In the first case, the Cubic Law (eq. 1) is mainly defined to estimate the permeability in fractured media (Witherspoon et al., 1980), since it considers a power relation between the permeability with the aperture. In the second case, Kozeny-Carman relation (eq. 2) is proposed to estimate based on the effective pore radius in granular media (Berry and Blair, 1987). In both cases, simplification must be considered, but the followed relations to calculate the fracture permeability (K_f, in m^2) are based on (Dippernaar and Van Rooy, 2016; Dvorkin, 2009):

$$K_f = \frac{\rho g e^3}{12 \mu b} \qquad \text{(eq.1)}$$

where ρ is the water density (in kg/m^3), g is the gravitational acceleration (in m/s^2), e is the aperture (in m) of the fracture, μ is the water dynamic viscosity (in kg/m×s), and b is the spacing between fractures (in m).

$$K_f = \frac{1}{K_c} \frac{\phi^3}{S^2 \tau^2} \qquad \text{(eq. 2)}$$

where ϕ is fraction volume of pore space, K_c is a constant related to pore geometry (where K_c=2 if the pore shape is assumed as cylindrical tube), S is the total surface area of the fractures, and τ is the tortuosity calculated from the ratio of length path (streamlines) determined in Paraview, in the same direction that the Lattice Boltzmann Method will be carried out.

Additionally, because the Cubic Law (eq. 1) required value of aperture (e), therefore to obtain a representative value of it we calculated the arithmetic, weighted, harmonic and geometric averages from the digital analysis in 2D (slice per slice) and 3D (whole volume).

3.3.2 Lattice Boltzmann Method (LBM)

The calculation by LBM is based on Darcy´s experiments, which simulates a viscous fluid flowing by the total segmented fracture (pore space) volume. A Parallel Lattice Boltzmann Solver was used considering a D3Q19 scheme and single-relaxation-time BGK (Bhatnagar-Gross-Krook) model, and this was implemented with the Palabos software (www.palabos.org). The result from the simulation is the permeability (K_f, in m^2) calculated as a function of the velocity magnitude of the flow, resolving the following equation (Eq. 3):

$$K_f = \frac{\mu\langle v\rangle}{\Delta P/\Delta L} \qquad \text{(eq. 3)}$$

where μ is the lattice viscosity (LB units), ⟨v⟩ is the mean fluid flow velocity (equivalent to Q/A, Darcy's velocity) through the fractured media, ΔP is the pressure gradient, and ΔL is the length of the sample.

The visualisation of the simulated models from LBM was by means of the Paraview software (Ayachit, 2015), which is an open-source and multi-platform software. Finally, and as indicated above, from the simulated models of permeability, through the tools of this software, the tortuosity (τ) was obtained from the ratio between the length of the streamlines with respect to the real length of the sample analysed.

4. RESULTS

4.1. Fracture digital features

The results about digital properties obtained from the segmentation of fractures are listed in Tables 2 and 3. The scans of artificially fractured samples show that only one fracture was developed in each of the analysed samples. Therefore, all results are referred exclusively due to the presence of this single fracture.

Fracture porosity (P_f, Table 2) show inverse relation with respect to temperature, decreasing the percentage. But in three conditions, samples presented a similar value of porosity, around 1.2 ±0.5%. The complexity of fractures is reflected in the different values in their superficial area (S, Table 2), but tortuosity shows that the pathways to the flow are very rectilinear because the mean values of τ (Table 2) are very close to 1. The minimum value is very similar for the three cases and a little more different from the maximum value, in which the unheated samples show "larger" tortuosity. In addition, it can be observed that with the increase in temperature, the difference between the minimum and the maximum value is minimized.

Table 2: Digital properties of the artificial fractures for non-heated (25 ºC) and heated (150 ºC and 210 ºC) samples. Legend: P_f, is the total fracture porosity (in %); S, is the total superficial area (in m^2); τ_f, is the tortuosity of the pathways through the fracture (dimensionless) and "mean", "min" and "max" are the averaged, minimum and maximum values for the tortuosity, respectively.

Sample	P_f	S	τ_f		
			mean	min	max
25 ºC	1.7	0.00101	1.10	1.03	1.30
150 ºC	1	0.03717	1.08	1.01	1.21
210 ºC	0.7	0.00566	1.07	1.02	1.12

The fracture aperture measured using the BoneJ plugin is showed in figure 2 and Table 3. Figure 2 shows the results in a histogram that this plugin drops immediately when the analysis ends. As can be see, the graphics present a distribution with ups and downs that correspond to odd and even values of the aperture (upper raw, Figure 2). For this in the bottom row is shown the normalised values of frequency (y-axis) versus aperture (x-axis).

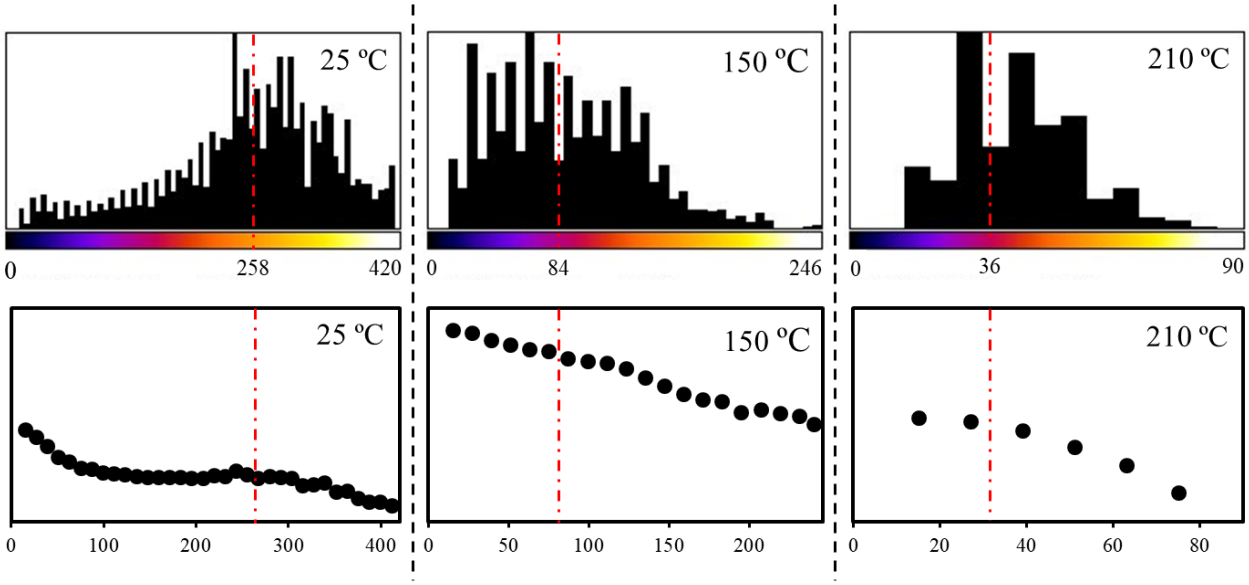

Figure 2: Fracture aperture distribution in 3D of each sample. In the upper row is shown the raw value directly obtained from BoneJ and in the bottom row, their respective normalised distribution. The value of aperture (x-axis) is expressed in μm, and the dotted red line indicates the averaged value offered by this method. In normalized distribution graphics the ordinate axis is at the same scale for both rows and in the y-axis is represented the frequency.

The averaged value of aperture from BoneJ is 258 μm, 84 μm and 36 μm for non-heated and heated samples at 150 ºC and 210 ºC, respectively. These values are calculated applying an arithmetic average over the measurements, as is indicated in the column "$\bar{x}_{arit}$" in Table 3 (e_f (3D). The other statistical estimation complemented by weighted, harmonic and geometric averages indicate that the values from weighted and geometric are more equilibrated because the effect of the weight of the number of extreme values of the very small and very large aperture is better compensated than by the other two methods.

On the other hand, comparing the calculated values for 2D and 3D, the weighted and geometric averaged values are very similar between them, but the geometry average presents a less deviation and similarity between its 2D and 3D aperture value.

Table 3: Results of bidimensional (2D) and three-dimensional (3D) analysis of the fracture aperture (e_f, *in μm*) from BoneJ plugin with different statistical approach. Legend: $\bar{x}$, is the mean value obtained by the arithmetic, weighted, harmonic and geometric averages and subscripted as "arit", "weig", "harm" and "geom", respectively.

	e_f (2D)				e_f (3D)			
	$\bar{x}_{arit}$	$\bar{x}_{weig}$	$\bar{x}_{harm}$	$\bar{x}_{geom}$	$\bar{x}_{arit}$	$\bar{x}_{weig}$	$\bar{x}_{harm}$	$\bar{x}_{geom}$
25 ºC	10	96	8	71	258	125	182	93
150 ºC	189	99	43	67	84	43	43	69
210 ºC	79	24	10	29	36	36	31	33

4.2. Permeability from Cubic Law, Kozeny-Carman Relation and Lattice-Boltzmann Method

Fracture permeabilities estimated from the Cubic Law and Kozeny-Carma relation are listed in Table 4. In the case of the Cubic Law, which is based on equation 1, it has been considered the fracture aperture calculated both for 2D as well as in 3D with BoneJ. However, this equation requires the value of b, the parameter related to the spacing between fractures per square meter. As in this case, the samples mechanically tested only had one fracture; hence, it was decided to use the simplified cubic law equation (Dippernaar and Van Rooy, 2016), which is:

$$K_f = \frac{ge^2}{12v} \qquad \text{(eq. 4)}$$

Therefore, with this new equation, the permeability can be calculated for only one fracture. The results obtained are very similar due to the used aperture is also very similar, so the permeability is in the same order of magnitude ($\approx\times10^{-9}$) regardless of the statistical method used for the fracture. Even, there is hardly any difference between the values calculated for digital analysis in 2D and 3D, nor has there been a clear difference between the non-heated and heated samples.

In the case of the calculations made using equation 2 (Kozeny-Carman relation), they show a clearer tendency about the heated samples respect to the fresh ones, since the samples without thermal treatment have values between 3 and 4 orders of magnitude above, from approximately $\times10^{-9}$ to $\times10^{-12/-13}$ m^2. In this sense, the percentage of porosity (P_f, Table 2) associated with the fractures

has been decisive more than the aperture (e_f, Table 3) and tortuosity (τ, Table 2), since both factors remained practically identical between the different samples.

Table 4: Estimated fracture permeability (K_f, in m^2) by means of Cubic Law, Kozeny-Carman relations and Lattice Boltzmann method. Legend: $\bar{x}$, is the mean value obtained by the arithmetic, weighted, harmonic and geometric averages and subscripted as "arit", "weig", "harm" and "geom", respectively; and "mean", "min" and "max" are then averaged, minimum and maximum values of tortuosity, respectively.

	Cubic Law (considering b = 0)								Kozeny-Carman relation			LBM
	K_f (2D)				K_f (3D)							
	$\bar{X}$arit	$\bar{X}$weig	$\bar{X}$harm	$\bar{X}$geom	$\bar{X}$arit	$\bar{X}$ weig	$\bar{X}$harm	$\bar{X}$geom	mean	min	max	K_f
25 ºC	9.2E-11	8.4E-09	5.9E-11	4.6E-09	6.0E-08	1.4E-08	3.0E-08	7.9E-09	2.0E-09	2.2E-09	1.4E-09	4.50E-11
150 ºC	3.3E-08	9.0E-09	1.7E-09	4.1E-09	4.1E-09	1.7E-09	1.7E-09	4.4E-09	3.1E-13	3.5E-13	2.8E-13	2.40E-11
210 ºC	5.7E-09	5.3E-10	9.2E-11	7.7E-10	1.2E-09	1.2E-09	8.8E-10	1.0E-09	4.6E-12	5.1E-12	4.2E-12	8.60E-13

Finally, the simulations in Palabos of the fluid flow through the fractures obtained intermediate values between those calculated by the Cubic Law and Kozeny-Carman relation, being around $\times 10^{-11}$ m^2, except to for the sample heated at 210 ºC which the permeability reaches the value of $\times 10^{-13}$ m^2 (LBM, Table 4). These pathways for the fluid flow can be graphically visualized on Paraview, and the trajectories are represented by streamlines for the samples (a, b and c, Figure 3), where the reddish and bluish colours indicate the points where the simulated flow has higher and lower velocity, respectively. In addition, these streamlines facilitate the observation of the tortuosity, as well as the effect of the roughness of the fracture. In this work, rugosity has not been directly taken into account, but given the nature of the LB method, it is implicitly considered, at least, to a greater extent regarding the calculations made with the Cubic Law and Kozeny-Carman relation.

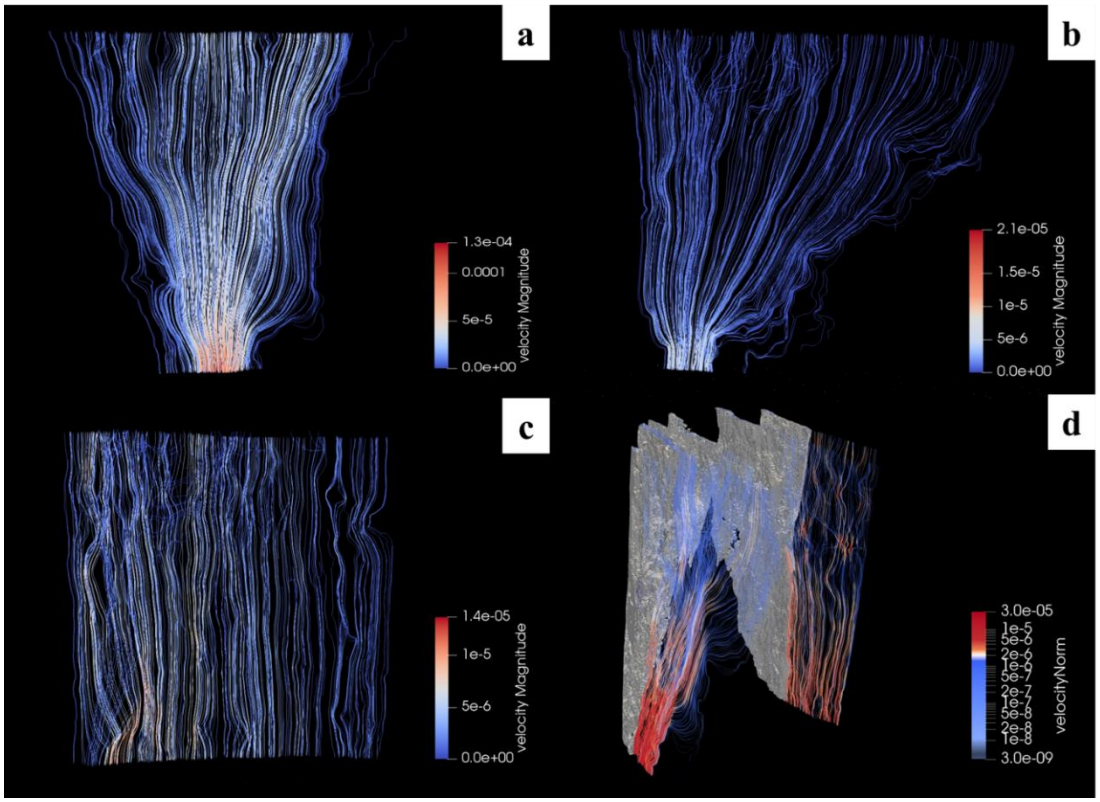

Figure 3: Simulated fluid flow by the artificial fractures on the non-heated sample (a) and heated at 150 ºC (b) and 210 ºC (c) samples. In (d) is shown an example of other sample heated at 150 ºC but with a network with multiple fractures.

5. DISCUSSION

The enhanced methodology by ADF did not allow to improve the segmentation about the possible thermal damage by the opened new cracks during the thermal treatment. However, the complementary petrophysical test which including water porosity, capillary coefficient and ultrasonic measurements showed that there was damage due to thermal stress since the values of porosity and capillarity increased while the speed of the ultrasonic waves decreased, as well as a decrease in the mechanical properties. The variation of all these petrophysical parameters is correlated with the effect of the increase in temperature on this rock (Molina et al., 2019). Therefore, since these thermal cracks cannot be detected, the permeability results shown here are only referred to the value given by the artificial fracture (fracture permeability) produced by mechanical failure. This is an aspect to consider because the matrix permeability can have an important effect on the total permeability and must be considered to the extrapolation to outcrop models or,

even, to the geothermal system. However, and based on both the values obtained in the petrophysical tests with respect to those obtained from the digital analysis on fractures, it is evident that the circulation of the hot fluids will be fundamentally conditioned through fractures than by the associated matrix porosity in this crystalline rock.

The permeability calculated in these heated and mechanically tested samples has increased by several orders of magnitude with respect to the value of fresh samples, which is, approximately, 6×10^{-19} m^2 (Sepúlveda, 2019). Specifically, fracture permeability obtained by the Cubic Law got the highest value ($K_f \approx \times10^{-9}$ m^2), meanwhile Lattice Boltzmann method offers an intermediate value ($K_f \approx \times10^{-11}$ m^2) and, finally, the Kozeny-Carman relation the lowest ($K_f \approx \times10^{-12/-13}$ m^2), but more similar to LBM. However, all these values are overestimated because other authors show that fractured natural systems hosted in granitic rocks have permeability values between $\times10^{-14}$ m^2 to $\times10^{-17}$ m^2 (Ingebritsen and Manning, 2010).

However, as mentioned above, the permeability value obtained by Cubic Law was without considering the parameter b and, consequently, using the simplified equation (eq. 4). Therefore, based on representative data of the spacing of the fractures in this granodiorite recorded in the field and hand samples, this outcrop shows a fracture density of 5 to 10 per square meter (Figure 4-a) and therefore an average spacing of 10 to 20 cm; while locally, this frequency of fractures can be higher. These fractures usually present apertures less than 1 mm and are quasi-rectilinear patterns at both the outcrop and the hand sample (Figure 4-b) scale, like those observed in the scanned samples.

Then, if the density of fractures (parameter b) recorded in the field and the aperture (e_f) of the digital analysis are introducing in eq. 1 of the Cubic Law, the new recalculated values are less overestimated and give similar results to those obtained in both LBM and Kozeny-Carman relation (Table 5). Now, the fracture permeability is ranging between $\times10^{-12}$ m^2 to $\times10^{-14}$ m^2.

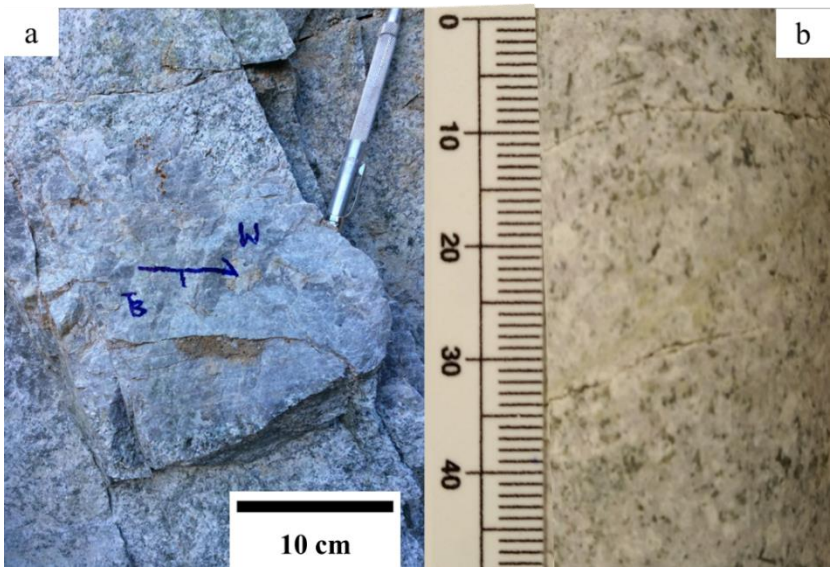

Figure 4: Examples of fracture distribution in the outcrop (≈ b is ranging between 10 to 20 cm) and in hand sample (≈ b is ranging between 1 to 5 cm).

In any of the three cases to estimate the permeability, it has been considered that the fractures are fully open so that the values obtained would be under the assumption of an ideal case where this fractures network would be very well connected and would be totally hydraulically conductive. However, in naturally fractured media, the conductivity can be affected, not only by the roughness of the fracture, but also by the partial or total filling by the precipitation of hydrothermal mineral phases, and also, by the connectivity of the network.

For all the above, the LB method is preset as a very good alternative for the estimation of permeability in fractures, since it considers all the geometric properties of these and not only the average value of the aperture or the porosity, and/or tortuosity. However, it is necessary to continue investigating the effect of these features on fracture permeability. In addition, in this work were only presented results of samples with a single artificial fracture, so it is also necessary to study how these properties and permeability vary in relation when there is more than one fracture, considering their interconnectivity, orientation, roughness, length, etc., as suggested the effect on the Cubic Law when the spacing values of the fracture network were introduced. About these considerations, in Figure 3-d is shown an example of a more complex fracture network than those presented in this work. This network is of a sample of the same granodiorite also heated to 150 °C and is currently under study to verify the implication of interconnection and complex networks in the permeability values obtained by LBM.

Table 5: Estimated fracture permeability (K_f, in m^2) by means of Cubic Law considering different values for the parameter "b" where values of 0.05, 0.1 and 0.2 indicate the spacing (in m) between fractures and are equivalent to 20, 10 and 5 fractures per square meter, respectively. For legend, see Table 4.

		k_f (2D)				k_f (3D)			
		$\overline{X}$arit	$\overline{X}$weig	$\overline{X}$harm	$\overline{X}$geom	$\overline{X}$arit	$\overline{X}$weig	$\overline{X}$harm	$\overline{X}$geom
"b" = 0.05	25 ºC	1.8E-14	1.6E-11	9.4E-15	6.6E-12	3.0E-10	3.6E-11	1.1E-10	1.5E-11
	150 ºC	1.2E-10	1.8E-11	1.5E-12	5.5E-12	5.5E-12	1.5E-12	1.5E-12	6.0E-12
	210 ºC	9.0E-12	2.5E-13	1.8E-14	4.5E-13	8.5E-13	8.5E-13	5.5E-13	6.6E-13
"b" = 0.1	25 ºC	9.2E-15	8.1E-12	4.7E-15	3.3E-12	1.5E-10	1.8E-11	5.5E-11	7.4E-12
	150 ºC	6.2E-11	8.9E-12	7.3E-13	2.8E-12	2.8E-12	7.3E-13	7.3E-13	3.0E-12
	210 ºC	4.5E-12	1.3E-13	9.2E-15	2.2E-13	4.3E-13	4.3E-13	2.7E-13	3.3E-13
"b" = 0.2	25 ºC	4.6E-15	4.1E-12	2.3E-15	1.6E-12	7.6E-11	8.9E-12	2.8E-11	3.7E-12
	150 ºC	3.1E-11	4.4E-12	3.6E-13	1.4E-12	1.4E-12	3.6E-13	3.6E-13	1.5E-12
	210 ºC	2.3E-12	6.3E-14	4.6E-15	1.1E-13	2.1E-13	2.1E-13	1.4E-13	1.6E-13

6. CONCLUSIONS

The main conclusions obtained by the digital analysis and digital rock model of artificially fractured granodiorite are:

The improvement of the images scanned by the application of the anisotropic diffusion filter has not allowed observing the cracks produced by thermal damage, even though complementary laboratory tests corroborate that this damage occurred. Therefore, this is more a limitation of the equipment than the method. However, the results obtained in the fractured samples have been improved, which has allowed a better segmentation of the fractures.

The digital analysis of fractures by means of X-Ray microComputed Tomography scans has allowed to measure one of the critical parameters for estimating permeability. This parameter has been the aperture of the fractures, and its distribution has been analysed both in 2D and 3D. The registered effect of increasing the temperature has produced a reduction in the aperture of the fracture and this difference shows that, independently of the method considered for the estimation of the permeability in fractures (Cubic Law, Kozeny-Carman relation or Lattice Boltzmann method), they give similar values to each other if the aspects of the fractures are taken into consideration such as density of fracture, aperture, tortuosity, etc. In addition, with the statistical analysis, for the averaging of the aperture with respect to the total fracture, the weighted and the geometric averages have presented the best values.

The calculations and the simulations have been carried out in samples with a single fracture, so the permeability with respect to the volume analysed is apparently overestimated. However, when considering the parameters of fracture density, the permeability is drastically reduced, and the values are close to those recorded in fractured natural systems. Therefore, we must continue to analyse the effect of more complex fracture networks for the circulation of fluids and be able to extrapolate these values to models closer to the reality of the Liquiñe geothermal system. These models must be supported with field data as well as additional tests in the laboratory applying other pressure and temperature conditions, as well as analysing the rest of the host rocks of this geothermal system. The integration of all this information could provide new data to understand how this geothermal system behaves in-depth due to the lack of wells or other methods which provide information.

ACKNOWLEDGEMENTS

This research was supported by projects FONDECYT Regular project Nº1180167 and FONDAP-CONICYT project N°15090013 "Centro de Excelencia en Geotermia de los Andes" (CEGA). X-ray micro Computed Tomography was founded by FONDEQUIP Project Nº EQM130028.

REFERENCES

Ayachit, U.: The ParaView Guide: A Parallel Visualization Application, Kitware, (2015), ISBN 978-1930934306.

Berry, J.C., and Blair, S.C.: Kozeny–Carman relations and image processing methods for estimating Darcy's constant, Journal of Applied Physics, 62, (1987), 2221-2228.

Cembrano, J., and Lara, L.: The link between volcanism and tectonics in the southern volcanic zone of the Chilean Andes: A review. Tectonophysics 471, (2009), 96–113.

Cid, H.E., Carrasco-Núñez, G., and Manea, V.C.: Improved method for effective rock microporosity estimation using X-ray microtomography. Micron 97, (2017), 11-21.

Cloetingh, S., and Van Wees, J.D.: Thermo-mechanical controls on geothermal energy resources: case studies in the Pannonian Basin and other natural laboratories. Acta Geodaetica et Geophysica 52, (2017), 157-160.

Dippernaar, M.A., and Van Rooy, J.L.: On the cubic Law and variably saturated flow through discrete open rough-walled discontinuities, International Journal of Rock Mechanics and Mining Sciences, 89, (2016), 200-211.

Dougherty, R.P., and Kunzelmann, K.H.: Computing Local Thickness of 3D Structures with ImageJ, *Proceedings*, Microscopy & Microanalysis Meeting, Ft. Lauderdale, Florida, (2007), Conference Presentation: http://www.optinav.com/LocalThicknessEd.pdf.

Dvorkin, J.: Kozeny-Carman Equation Revisited, (2009).

Ebigbo, A., Niederau, J., Marquart, G., Dini, I., Thorwart, M., Rabble, W., Peching, R., Bertani, R., Clauser, C.: Influence of depth, temperature, and structure of a crustal heat source on the geothermal reservoirs of Tuscany: numerical modelling and sensitivity study, Geothermal Energy, 4, (2016), 1-29.

Griffiths, L., Heap, M.J., Baud, P., Schmittbuhl, J.: Quantification of microcrack characteristics and implications for stiffness and strength of granite. International Journal of Rock Mechanics and Mining Sciences, 100, (2017), 138-150.

Gudmundsson, A. Rock fractures in geological processes. Cambridge: Cambridge University Press, (2011), doi:10.1017/CBO9780511975684.

Held, S., Schill, E., Schneider, J., Nitschke, F., Morata, D., Neumann, T., Kohl, T.: Geochemical characterization of the geothermal system at Villarrica volcano, Southern Chile; Part 1: Impacts of lithology on the geothermal reservoir. Geothermics 74, (2018), 226-239.

Hommel, J., Coltman, E., and Class, H.: Porosity-permeability relations for evolving pore space: a review with a focus on (bio-) geochemically altered porous media, Transport in Porous Media, 124, (2018), 589-629.

Ingebritsen, S.E., and Manning, C.E.: Permeability of the continental crust: dynamic variations inferred from seismicity and metamorphism, Geofluids, 10, (2010), 193-205.

Lara, L., and Moreno, H.: Geología del área Liquiñe - Neltume, regiones de La Araucanía y de Los Lagos, Escala 1:100.000. Carta Geológica de Chile, Serie Geología Básica n.83, (2004), SERNAGEOMIN, Santiago, Chile.

Molina, E., Arancibia, G., Sepúlveda, J., Roquer, T., Mery, D., Morata, D.: Digital rock approach to model the permeability in an artificially heated and fractured granodiorite from the Liquiñe Geothermal System (39ºS), Rock Mechanics and Rock Engineering (under review, 2019).

Pérez-Flores, P., Cembrano, J., Sánchez-Alfaro, P., Veloso, E., Arancibia, G., and Roquer, T.: Tectonics, magmatism and paleo-fluid distribution in a strike-slip setting: Insights from the northern termination of the Liquiñe–Ofqui fault System, Chile. Tectonophysics 680, (2016), 192-210.

Rosenau, M., Melnick, D., and Echtler, H. Kinematic constraints on intra-arc shear and strain partitioning in the southern Andes between 38°S and 42°S latitude. Tectonics, 25(4), (2006). https://doi.org/10.1029/2005TC001943

Sánchez, P., Pérez-Flores, P., Arancibia, G., Cembrano, J., Reich, M.: Crustal deformation effects on the chemical evolution of geothermal systems: the intra-arc Liquiñe–Ofqui fault system, Southern Andes. International Geology Review, 55, (2013), 1384-1400.

Schindelin, J., Arganda-Carreras, I. & Frise, E.: Fiji: an open-source platform for biological-image analysis". Nature methods 9, (2012), 676-682, PMID 22743772, doi:10.1038/nmeth.2019. Software version 1.52b.

Sepúlveda, J.: Thermo-mechanical behavior of the granodiorite at the Liquiñe fractured geothermal system (39ºS), related to fault system in the Southern Volcanic Zone. Unpublished master's thesis, G. Arancibia (Adv.), (2019), Pontificia Universidad Católica de Chile, Santiago, Chile.

Violay, M., Heap, M.J., Acosta, M., Madonna, C.: Porosity evolution at the brittle-ductile transition in the continental crust: Implications for deep hydro-geothermal circulation. Scientific Reports 7, (2017), 1-10.

Witherspoon, P.A., Wang, J.S.Y., Iwai, K., and Gale, J.E.: Validity of cubic law for fluid-flow in a deformable rock fracture, Water Resources Research, 16, (1980), 1016-1024.

Yang, Y., Lui, Z., yao, J., Zhang, L., Ma, J., Hejazi, S.H., Luquot, L., and Ngarta, T.D.: Flow simulation of artificially induced microfractures using digital rock and Lattice Boltzmann Methods, Energies, 11, (2018), 2145, 1-17.